



Extending radially self-similar MHD models by introducing an outer disk radius

MATTHIAS STUTE¹, KANARIS TSINGANOS¹, NEKTARIOS VLAHAKIS¹, TITOS MATSAKOS², AND JOSE GRACIA³

¹ IASA AND SECTION OF ASTROPHYSICS, ASTRONOMY AND MECHANICS, DEPARTMENT OF PHYSICS, UNIVERSITY OF ATHENS, PANEPISTIMIOPOLIS, 157 84 ZOGRAFOS, ATHENS, GREECE

² DIPARTIMENTO DI FISICA GENERALE, UNIVERSITÀ DEGLI STUDI DI TORINO, VIA PIETRO GIURIA 1, 10125 TORINO, ITALY

³ SCHOOL OF COSMIC PHYSICS, DUBLIN INSTITUTE OF ADVANCED STUDIES, 31 FITZWILLIAM PLACE, DUBLIN 4, IRELAND



Introduction

- Astrophysical jets are ubiquitous, occurring in a variety of objects on very different size and mass scales: AGN, XRBs, Symbiotic Stars and YSOs.
- In all such cases, jets and disks seem to be inter-related. Disks provide the jets with the ejected plasma and magnetic fields and jets are possibly the most efficient sink of excess angular momentum in the disk (e.g. Ferreira 2007) making the accretion possible in the first place.
- The magnetic model of a disk-wind seems to explain simultaneously acceleration, collimation as well as the observed high jet speeds (Königl & Pudritz 2000).

Self-similar jet formation models and their limitations

- The first analytical work studying magneto-centrifugal acceleration along magnetic field lines threading an accretion disk was done by Blandford & Payne (1982). They have shown the braking of matter in azimuthal direction inside the disk and their acceleration above the disk surface by the poloidal magnetic field components. Toroidal components of the magnetic field then collimate the flow.
- Numerous semi-analytic models extended the work of Blandford & Payne (1982) along the guidelines of radially self-similar solutions of the full magnetohydrodynamics (MHD) equations (Vlahakis & Tsinganos 1998).
- The model of Blandford & Payne (1982) had one serious drawback, self-similar analytical models in general have two more limitations: I. The outflow speed at large distances does not cross the corresponding limiting characteristic, with the result that the terminal wind solution is not causally disconnected from the disk. II. Singularities exist at the jet axis in radially self-similar models. III. No intrinsic scale exists, the jets formally extend to radial infinity.
- Several steps were done to solve these problems: I. Vlahakis et al. (2000) showed that a terminal wind solution can be constructed which is causally disconnected from the disk. II. Numerical simulations are necessary to extend the analytical solutions, as it has been done within the JETSET network by Gracia et al. (2006) and Matsakos et al. (2007). III. The aim of this project now is to investigate numerically, how imposing an outer radius of the jet, i.e. cutting off the analytical solution at arbitrary radii, affects the topology and structure, the stability and ability to explain observations of a radial self-similar analytical solution.

Theoretical framework

- The ideal time-dependant MHD equations which are solved are

$$\begin{aligned} \frac{\partial \rho}{\partial t} + \nabla \cdot (\rho \vec{v}) &= 0 \\ \frac{\partial \vec{v}}{\partial t} + (\vec{v} \cdot \nabla) \vec{v} + \frac{1}{\rho} \vec{B} \times (\nabla \times \vec{B}) + \frac{1}{\rho} \nabla p &= -\nabla \Phi \\ \frac{\partial p}{\partial t} + \vec{v} \cdot \nabla p + \Gamma p \nabla \cdot \vec{v} &= \Lambda \\ \frac{\partial \vec{B}}{\partial t} - \nabla \times (\vec{v} \times \vec{B}) &= 0 \end{aligned}$$

where ρ , p , \vec{v} , \vec{B} , $\Phi = -\mathcal{G}M/r$ denote the density, pressure, velocity, magnetic field over $\sqrt{4\pi}$ and the gravitational potential of the central object with mass M , Λ represents the volumetric energy gain/loss term. r is the spherical radius, R the cylindrical radius.

- By assuming steady-state and axisymmetry, several conserved quantities exist along the fieldlines (Tsinganos 1982):

$$\Psi_A(A) = \frac{\rho \vec{v}_\phi}{B_\phi} \quad \Omega(A) = \frac{1}{R} \left(v_\phi - \frac{\Psi_A B_\phi}{\rho} \right) \quad L(A) = R v_\phi - \frac{R B_\phi}{\Psi_A}$$

where $A = (1/2\pi) \int \vec{B}_\phi \cdot d\vec{S}$ is the magnetic flux function, Ψ_A the mass-to-magnetic-flux ratio, Ω the field angular velocity, and L the total specific angular momentum. The ratio $\sqrt{L/\Omega}$ defines the Alfvénic lever arm, R_* , along the reference fieldline at the point where the flow speed is equal to the poloidal Alfvénic one. In the adiabatic-isentropic case ($\Lambda = 0$), there exist two more integrals, the total energy flux density to mass flux density E and the specific entropy Q , which are given by:

$$E(A) = \frac{v^2}{2} + \frac{\Gamma}{\Gamma-1} \frac{p}{\rho} + \Phi - \Omega R \frac{B_\phi}{\Psi_A} \quad Q(A) = \frac{p}{\rho^\Gamma}$$

- We use the steady, radially self-similar solution which is described in Vlahakis et al. (2000) and crosses successfully all three critical surfaces providing the key functions $M(\theta)$ (Alfvénic Mach number), $G(\theta)$ (cylindrical distance in units of the corresponding Alfvénic lever arm) and $\psi(\theta)$ (angle between a particular poloidal fieldline and the cylindrical radial direction). Then, the fieldlines can be labeled by

$$A = \frac{B_* R_*^2}{x} \alpha^{x/2}, \quad \text{with} \quad \alpha = \frac{R^2}{R_*^2 G^2}$$

and the physical variables can be constructed as follows (Vlahakis et al. 2000)

$$\begin{aligned} \rho &= \rho_* \alpha^{x-3/2} \frac{1}{M^2} & p &= p_* \alpha^{x-2} \frac{1}{M^{2\gamma}} \\ \vec{v}_\phi &= -v_* \alpha^{-1/4} \frac{M^2}{G^2} \frac{\sin \theta}{\cos(\psi + \theta)} (\cos \psi \vec{e}_R + \sin \psi \vec{e}_z) \\ \vec{B}_\phi &= -B_* \alpha^{x/2-1} \frac{1}{G^2} \frac{\sin \theta}{\cos(\psi + \theta)} (\cos \psi \vec{e}_R + \sin \psi \vec{e}_z) \\ v_\phi &= v_* \lambda \alpha^{-1/4} \frac{G^2 - M^2}{G(1 - M^2)} & B_\phi &= -B_* \lambda \alpha^{x/2-1} \frac{1 - G^2}{G(1 - M^2)} \end{aligned}$$

x is a model parameter governing the scaling of the magnetic field. The starred quantities are related to their characteristic values at the Alfvén radius R_* along the reference fieldline $\alpha = 1$. They are interconnected with the following relations:

$$v_* = \frac{B_*}{\sqrt{\rho_*}} \quad p_* = \frac{\beta B_*^2}{2} \quad \mathcal{K} = \sqrt{\frac{\mathcal{G}M}{R_* v_*^2}}$$

where \mathcal{G} and \mathcal{M} are the gravitational constant and the mass of the central object respectively. The constants λ and \mathcal{K} are the specific angular momentum of the flow in units of $v_* R_*$ of the reference fieldline and the Keplerian velocity at distance R_* measured on the disk in units of v_* , respectively. Finally β is the ratio of gas pressure to magnetic pressure and is proportional to the gas entropy.

General numerical setup

- We solve the MHD equations with the PLUTO code (Mignone et al. 2007).
- We define the reference length R_* to be unity, while the reference velocity is normalized by setting $v_* = 1$. Time is given in units of $t_0 = 2\pi \sqrt{R_*^3/\mathcal{G}M}$, i.e. one Keplerian orbit at $R_* = 1$. The model parameters of this solution were chosen as $x = 0.75$ and $\gamma = 1.05$, while the solution parameters are given to be $\lambda = 11.70$, $\beta = 2.99$, $\mathcal{K} = 2.00$, corresponding to the solution in Vlahakis et al. (2000) crossing all critical points.
- We divide our computational domain in a jet region and an external region, which are separated by a truncation field line α_{trunc} . For smaller values of α – i.e. smaller radii – our initial conditions are fully determined by the solution of Vlahakis et al. (2000). The way the external region should be initialized, however, is not as obvious:
 - How is the choice of α_{trunc} affecting the results?
 - What are the effects of numerical resolution and domain size?
 - What are the consequences of different initializations of the external region?
- We impose axisymmetry at the axis and outflow conditions at the top z boundary. At the outer radial boundary, we apply outflow conditions. At the lower boundary, we keep the quantities fixed to their analytical values, however, making sure that they are not over-specified. Thus the number of quantities set by the analytical solution is decreasing by one when a critical surface is crossed for increasing R (for details, see Matsakos et al. 2007).

Test simulations

- We have run ten models, together with the unchanged model of Vlahakis et al. (2000). We run several models where the analytical solution is truncated at different α_{trunc} and where the external region is initialized differently (with constant values, with the analytical solution where ρ and v_z are damped with $\alpha_{\text{trunc}}/\alpha$, where only v_z is set to a smaller value or where all quantities are damped with an exponential factor).
- The basic evolution is similar in most models and can be divided into four phases:
 1. A shock front starting at the jet base runs across the jet, bending its outer surface and forming a dent which then travels out and upwards. This front is not present also in the analytical reference model 2DB of Matsakos et al. (2007).
 2. Behind the dent, a new smooth jet surfaces develops with a larger radius than the initial one. This configuration stays for several t_0 in the models.
 3. The outer medium compresses the jet along its full length, pinching it even close to the rotation axis at certain z values. Here very dense knots are formed.
 4. The jet material pushes back and a more or less stationary topology is established with an almost constant jet radius along the jet.
- **The only model without this collapse is the models where all quantities are damped with an exponential factor. Thus it seems to be imperative that also the external region is close to equilibrium.**

Science simulations

- In the science models, we use a different approach: we initialize the external region with another analytical solution with slightly changed parameters. From Vlahakis et al. (2000), one can show that if we start with a steady analytical solution with the variables ρ , p , \vec{v} , \vec{B} , then one can easily construct a second steady solution by setting

$$\begin{aligned} R' &= \lambda_1 R & Z' &= \lambda_1 Z & \vec{B}' &= \lambda_2 \vec{B} & \vec{v}' &= \sqrt{\frac{\lambda_3}{\lambda_1}} \vec{v} \\ \rho' &= \frac{\lambda_1 \lambda_2^2}{\lambda_3} \rho & p' &= \lambda_2^2 p & \mathcal{M}' &= \lambda_3 \mathcal{M} \end{aligned}$$

Since in our case, both solutions should have the same central object, we set $\lambda_3 = 1$. We match both solutions by using the function

$$Q = Q_{\text{jet}} \exp[-(\alpha/\alpha_{\text{trunc}})^2] + Q_{\text{ext}} (1 - \exp[-(\alpha/\alpha_{\text{trunc}})^2])$$

- for all quantities. The successful test model is equivalent to $Q_{\text{ext}} = 0$.
- In model SC1, we try to mimic the behavior of the successful test model with $Q_{\text{ext}} = 0$ by setting $\lambda_1 = 10^3$ and $\lambda_2 = 10^{-3}$ ($v' = 10^{-3/2} v$, $B' = 10^{-3} B$, $p' = 10^{-6} p$, $\rho' = 10^{-3} \rho$). In model SC2, we use $\lambda_1 = 100$ and $\lambda_2 = 0.1$ (case 3), i.e. $v' = 0.1 v$, $B' = 0.1 B$, $p' = 0.01 p$, $\rho' = \rho$, in the exterior region and in model SC3 in the interior. In model SC4, our combination is $\lambda_1 = 1$ and $\lambda_2 = 0.1$ (case 1.) in the exterior and in model SC5 in the interior, leading to $v' = v$, $B' = 0.1 B$, $p' = 0.01 p$, $\rho' = 0.01 \rho$.
- A more realistic model should have a higher pressure and/or magnetic field outside ($\lambda_2 > 1$) and higher velocity inside ($\lambda_1 > 1$). However, a higher density inside is not possible then ($\lambda_1 \lambda_2^2 \gg 1$). Thus we abandon the analytical solution in the exterior region and add additional pressure. In model SC6, we use $\lambda_1 = 10^3$ and $\lambda_2 = 10^{-3}$ as in model SC1, however, we keep the thermal pressure of the unchanged analytical solution and add the magnetic pressure which is lost by damping the magnetic field components.

References

- Blandford R. D., Payne D. G. 1982, MNRAS, 199, 883
 Ferreira, J. 2007, in: "Jets from Young Stars: Models and Constraints", Lecture Notes in Physics, Vol. 723; Ferreira, J.; Dougados, C.; Whelan, E. (Eds.)
 Gracia J., Vlahakis N., Tsinganos K. 2006, MNRAS, 367, 201
 Königl A., Pudritz R. E. 2000, in Mannings V., Boss A.P., Russell S. S., eds, Protostars and Planets IV. Univ. Arizona Press, Tucson, p. 759
 Matsakos T., Tsinganos K., Vlahakis N., Massaglia S., Mignone A., Trussoni E. 2007, A & A accepted, arXiv:0710.3406
 Mignone, A., Bodo, G., Massaglia, S., et al. 2007, ApJS, 170, 228
 Tsinganos, K. C. 1982, ApJ, 252, 775
 Vlahakis N., Tsinganos K. 1998, MNRAS, 298, 777
 Vlahakis N., Tsinganos K., Sauty C., Trussoni E. 2000, MNRAS, 318, 417

The present work is supported by the European Community's Marie Curie Actions - Human Resource and Mobility within the JETSET (Jet Simulations, Experiments and Theory) network under contract MRTN-CT-2004 005592.

Results of the simulations

Flow structure

- The flows behave qualitatively very different, depending on whether the scaled-down solution is outside or inside the original one. In the first case, the opening angle of the flow increases until a new equilibrium is established. The final opening angles, however, are too large for a collimated jet (47 – 58° in models SC1, SC2, SC4 and SC6). In the second case, the opening angle decreases to very small final opening angles (3 – 5° in models SC3 and SC5). The decrease of the opening angle by the lack of support against the external pressure creates several shocks travelling outwards in the exterior region.

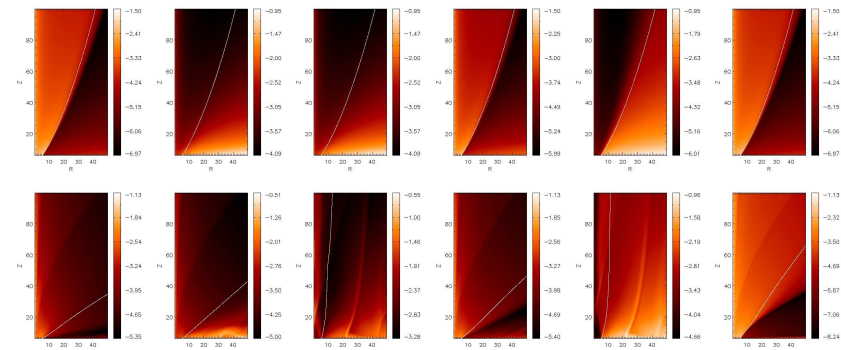


Figure 1: Structure of the flow for models SC1 – SC6 at timesteps $t = 0 t_0$ (top) and $t = 50 t_0$ (bottom), respectively. Also plotted is the magnetic fieldline anchored in the lower boundary where $\alpha = 0.4$ (white line)

Jet radii and temporal evolution

- The final equilibrium is reached in all models within about 10 t_0 and stays stable for 50 t_0 . In model SC4, a glitch can be seen where the jet radius changes suddenly (presumably caused by boundary effects), however, after that the radius remains constant again for another 20 t_0 .

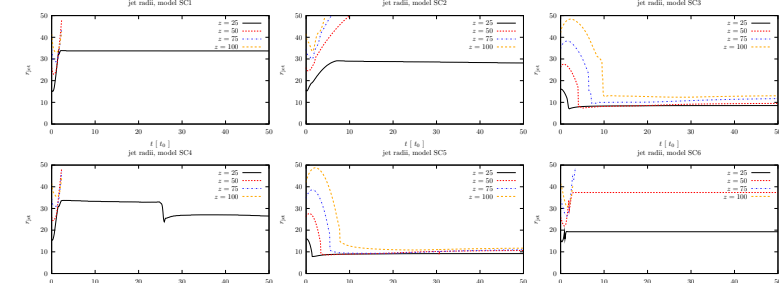


Figure 2: Evolution of the jet radius measured with the fieldline plotted in previous figures for models SC1 – SC6 at several z values above the equatorial plane

Flow profiles

- The initial profile follows the analytical solution in the interior region and is damped in the exterior (in models SC1, SC2 and SC4) and vice versa (in models SC3 and SC5).
- In the first case, the final solution seems to converge to another analytical solution different from the initial one. At large radii, most profiles have a similar shape than the unchanged analytical solution, we started with. At small radii ($R < 5$), however, the final solution deviates drastically, which, however, is expected, since the analytical solution is modified close to the axis to avoid the intrinsic singularities as in Gracia et al. (2006) and Matsakos et al. (2007).
- In the second case, the initial profiles have to be changed dramatically to stop the decrease of the opening angle and the collapse of the jet. This is done by creating large magnetic pressure at $R < 10$, the thermal pressure profile is not very different from the analytical one. The profile of the R velocity component is almost constant around $v_R = 0$.

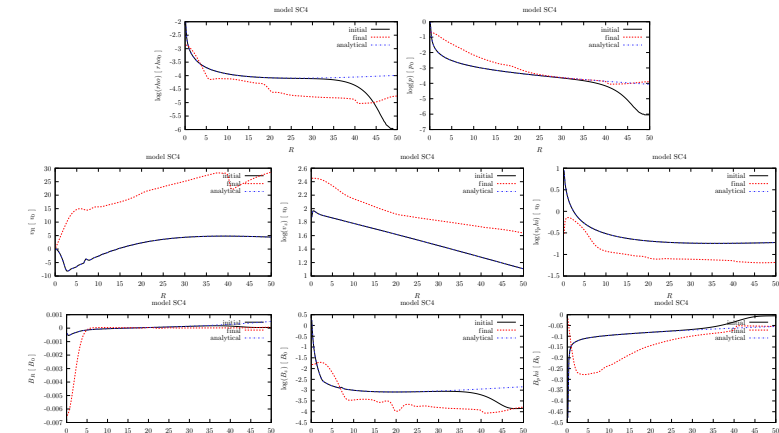


Figure 3: Quantities at the outer axial boundary in model SC4: density, pressure, velocity components in R , z and ϕ , magnetic field components in R , z and ϕ ; given are the initial profiles (black), the final profiles (red) and the profiles in the unchanged analytical solution of Vlahakis et al. (2000) (blue)

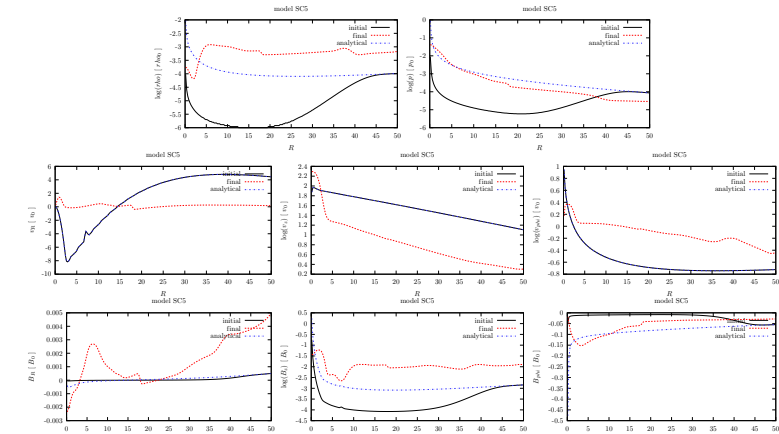


Figure 4: Quantities at the outer axial boundary in model SC5: density, pressure, velocity components in R , z and ϕ , magnetic field components in R , z and ϕ ; given are the initial profiles (black), the final profiles (red) and the profiles in the unchanged analytical solution of Vlahakis et al. (2000) (blue)

Discussion

- We find stationary two-component solutions where an unchanged and a scaled-down analytical solution of Vlahakis et al. (2000) are matched.
- The boundary between both solutions is always shifted towards the solution with reduced quantities. Especially, the reduced thermal and magnetic pressure change the perpendicular force balance at the "surface" of the flow.
- In the models where the scaled-down analytical solution is *outside* the unchanged one, the inside solution converges to another analytical solution with different parameters.
- In the models where the scaled-down analytical solution is *inside* the unchanged one, the whole two-component solution changes dramatically to support the flow from collapsing totally to the symmetry axis.